

DYNAMIC FUNCTIONAL CONNECTIVITY USING HEAT KERNEL

Shih-Gu Huang^{*} Moo K. Chung^{*} Ian C. Carroll[‡] H. Hill Goldsmith[‡]

^{*} Department of Biostatistics and Medical Informatics, University of Wisconsin, Madison, USA

[‡] Waisman Center & Department of Psychology, University of Wisconsin, Madison, USA

ABSTRACT

Sliding and tapered sliding window methods are the most common approaches in computing dynamic correlations between brain regions. However, due to data acquisition and physiological artifacts in resting-state fMRI, the sidelobes of the window functions in spectral domain will cause high-frequency fluctuations in dynamic correlations. To address the problem, we propose to define the heat kernel, a generalization of the Gaussian kernel, on a circle continuously without boundary. The windowless dynamic correlations are then computed by the weighted cosine series expansion, where the weights are related by the heat kernel. The proposed method is applied to the study of dynamic interhemispheric connectivity in the human brain in identifying the state space more accurately than the existing window methods.

Index Terms— Dynamic functional brain connectivity, windowless dynamic correlation, heat kernel, sliding window method, resting state fMRI

1. INTRODUCTION

The windowed dynamic correlation is one of popular approaches to estimate dynamically changing functional brain connectivity [1, 2]. The sliding window (SW) method using a square window [3, 4, 5] is the most commonly used windowed methods. To remedy the zig-zag patterns in SW method caused by the use of square windows, the tapered sliding window (TSW) [4, 6] Hamming window [7] and Tukey window [8] methods were proposed. However, the sidelobes of the window functions in spectral domain [9] will cause high-frequency fluctuations in the dynamic correlations in all these methods. Instead of using a window function with finite support, we propose to use the heat kernel in computing dynamic correlations over the whole domain of the data. We show that the heat kernel method is better than the SW and TSW-methods with respect to the underlying state space. The main contributions of the paper are as follows. 1) We present a novel technique to compute the dynamic correlations without finite windows that cause the zig-zag patterns. 2) The proposed method is applied in determining the state space

in the dynamic interhemispheric connectivity of resting-state fMRI.

2. METHODS

2.1. Heat kernel convolution on a circle

Diffusion on [0, 1]. Consider 1D heat diffusion of time series data $f(t)$ on unit interval $[0, 1]$:

$$\frac{\partial}{\partial s} h(t, s) = \frac{\partial^2}{\partial t^2} h(t, s) \quad (1)$$

at diffusion time s with initial condition $h(t, s = 0) = f(t)$. The unique solution is given by the weighted cosine series representation [11]

$$h(t, s) = \sum_{l=0}^{\infty} e^{-l^2 \pi^2 s} c_{fl} \psi_l(t), \quad c_{fl} = \int_0^1 f(t) \psi_l(t) dt \quad (2)$$

where $\psi_0(t) = 1$, $\psi_l(t) = \sqrt{2} \cos(l\pi t)$ are the cosine basis and c_{fl} are the cosine series coefficients of f .

Diffusion on a circle. To avoid the boundary effect in SW- and TSW-methods [10], we project $f(t)$ onto the circle by connecting its mirror reflection in the following way:

$$g(t) = f(t) \text{ if } t \in [0, 1], \quad g(t) = f(2 - t) \text{ if } t \in [1, 2]$$

Then g is a periodic function defined on the circle \mathcal{C} with circumference 2. Then we solve (1) with initial condition $h(t, s = 0) = g(t)$ on circle \mathcal{C} . It can be shown that solution is given by

$$h(t, s) = \int_0^1 K_s(t, t') f(t') dt', \quad (3)$$

where heat kernel $K_s(t, t')$ is given by

$$K_s(t, t') = \sum_{l=0}^{\infty} e^{-l^2 \pi^2 s} \psi_l(t) \psi_l(t'). \quad (4)$$

The parameter s is the bandwidth of the heat kernel and controls the amount of diffusion. Unlike window functions, there

Correspondence should be sent to Huang (shihgu@gmail.com) or Chung (mkchung@wisc.edu).

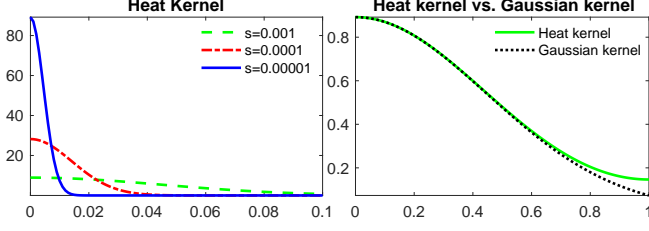


Fig. 1. Left: heat kernels $K_s(t, t')$ at $t = 0$ with diffusion time or bandwidth s . Right: The heat kernel with $s = 0.1$ has thicker tails compared to the Gaussian kernel of same FWHM.

is no endpoint or boundary in the heat kernel defined on a circle. On the circle, which is a curved manifold, heat kernel has a thicker tail compared to truncated Gaussian kernel (Figure 1). As bandwidth s increases, the tail regions get thicker and eventually we have $\lim_{s \rightarrow \infty} K_s(t, t') = 1/2$ [12].

2.2. Windowless dynamic correlation

For time series data $x(t)$ and $y(t)$ in interval $[0, 1]$, instead of using square window, we propose to use generalized kernel $w(t, t')$ satisfying $\int_0^1 w(t, t') dt' = 1$ for any t . The data will be mirror reflected to form periodic data on circle \mathcal{C} . With the normalized kernel, we define the windowless dynamic correlation between $x(t)$ and $y(t)$ as

$$r_{x,y}(t) = \frac{\int_0^1 w(t, t') x(t') y(t') dt' - \mu_x(t) \mu_y(t)}{\sigma_x(t) \sigma_y(t)}, \quad (5)$$

where $\mu_x(t) = \int_0^1 w(t, t') x(t') dt'$ and

$$\sigma_x^2(t) = \int_0^1 w(t, t') x^2(t') dt' - \mu_x^2(t)$$

are the dynamic mean and variance of $x(t)$. $\mu_y(t)$ and $\sigma_y^2(t)$ are defined similarly. Due to the symmetry, the integral is not taken over the circle \mathcal{C} , i.e., $[0, 2]$.

Suppose c_{xl} , c_{yl} , c_{xyl} , c_{xxl} and $c_{yy l}$ denote the cosine series coefficients of $x(t)$, $y(t)$, $x(t)y(t)$, $x(t)x(t)$ and $y(t)y(t)$ in representing them as, for instance,

$$x(t) = \sum_{l=0}^{\infty} c_{xl} \psi_l(t), \quad x(t)y(t) = \sum_{l=0}^{\infty} c_{xyl} \psi_l(t).$$

If we use heat kernel $w(t, t') = K_s(t, t')$, correlation (5) can be written as

$$r_{x,y}(t) = \frac{\sum_{l=0}^{\infty} e^{-l^2 \pi^2 s} c_{xyl} \psi_l(t) - \mu_x(t) \mu_y(t)}{\sigma_x(t) \sigma_y(t)},$$

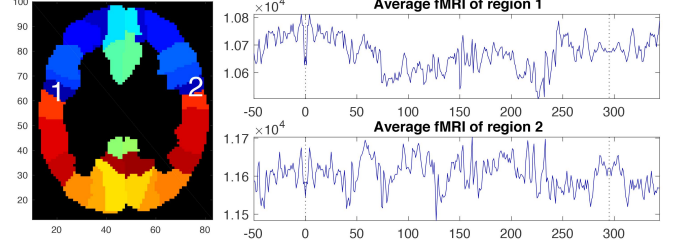


Fig. 2. Left: brain parcellation using AAL template. The hemispherically paired brain regions are displayed with the same color. Right: average fMRI signals within left (region 1) and right (region 2) precentral gyri.

with

$$\begin{aligned} \mu_x(t) &= \sum_{l=0}^{\infty} e^{-l^2 \pi^2 s} c_{xl} \psi_l(t), \\ \sigma_x^2(t) &= \sum_{l=0}^{\infty} e^{-l^2 \pi^2 s} c_{xxl} \psi_l(t) - \mu_x^2(t). \end{aligned}$$

In numerical implementation, the coefficients c_{xxl} , $c_{yy l}$ and c_{xyl} can be obtained from c_{xl} and c_{yl} through the convolution theory of cosine series. Then (5) can be computed using only the c_{xl} and c_{yl} coefficients, which are estimated via the least squares method [11].

3. APPLICATION

3.1. Resting-state fMRI data and preprocessing

Resting-state (rs) functional magnetic resonance images (rs-fMRI) were collected on a 3T MRI scanner (Discovery MR750, General Electric Medical Systems, Milwaukee, WI, USA) with a 32-channel RF head coil array. T1-weighted structural images (1 mm³ voxels) were also acquired axially with an isotropic 3D Bravo sequence (TE = 3.2 ms, TR = 8.2 ms, TI = 450 ms, flip angle = 12°). The functional scans were undergone a series of data reduction, correction, registration, and spatial and temporal preprocessing [13]. The resulting rs-fMRI consists of 91 × 109 × 91 isotropic voxels at 295 time points. Excluding one subject that has no fMRI signals in two brain regions, the average fMRI signals of 479 healthy subjects ranging in age from 13 to 25 years were used in our study.

We employed the Automated Anatomical Labeling (AAL) brain template to parcellate the brain volume into 116 non-overlapping anatomical regions [14]. The fMRI data were averaged across voxels within each brain region resulting in 116 average fMRI signals with 295 time points for each subject. Figure 2 displays two representative average fMRI at two brain regions.

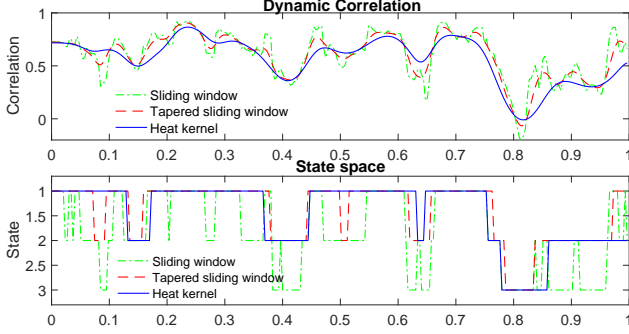


Fig. 3. Dynamic correlations (top) between the average fMRI signals of left and right precentral gyri and the corresponding state space (bottom) using the SW-, TSW- and heat kernel methods.

3.2. Dynamic interhemispheric connectivity

For each subject, the 116 averaged rs-fMRI signals were scaled to fit to unit interval $[0, 1]$. To reduce the boundary effect, we continuously connected fMRI with its mirror reflection at the end points $t = 0$ and $t = 1$. Figure 2 displays the rs-fMRI in the left and right precentral gyri connected at the first ($t = 0$) and the 295-th scan ($t = 1$). This has the effect of making fMRI a circular data on a circle with circumference 2. Excluding the 8 vermis regions that do not belong to the left or right brain hemisphere, we computed the 54 dynamic interhemispheric correlations from the remaining 108 fMRI time series.

In previous studies [4, 6], square window of size 22 TRs convolved with a Gaussian kernel with bandwidth 3 TRs was used in the TSW-method. Following the literature, the SW-method with size 22 TRs and heat kernel method with bandwidth $s = 5 \times 10^{-4}$ (FWHM 22 TRs) were used in this study.

Figure 3 displays the result of the dynamic correlation between the left and right precentral gyri using the three methods. The SW-method shows the severe zig-zag pattern caused by the introduction of discrete window. The TSW-method was able to remedy such zig-zag patterns but still showing rapid changes from one time point to the next. On the other hand, the heat kernel method has much fewer high-frequency fluctuations and estimates the correlation more smoothly over time, which is biologically more realistic.

3.3. Estimation of distinct state space

Rs-fMRI exhibits three distinct transient connectivity patterns that repetitively occur throughout the time course [15]. These discrete states serve as the basis of investigating brain connectivity. They are reliably observed across different subjects, groups and sessions [16, 17]. It has been shown that additional measure of the fluctuations from one state to the next state provides meaningful between-group variations [1, 18] and clinical status [19] and can be used as a potential

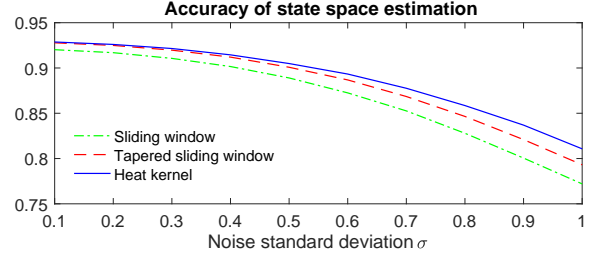


Fig. 4. Accuracy of state space estimation of the SW-, TSW- and heat kernel methods for different standard deviation σ of noise. Average of 100 independent simulations was plotted.

biomarker for future studies. Such state spaces were first identified using the k -means clustering [4] and subsequently adopted by many others as the standard baseline method [1, 20, 5, 19].

In this study, we apply the baseline k -means clustering to identify the distinct states in interhemispheric connectivity and compare the performance of the proposed method against the SW- and TSW-methods. For each interhemispheric pair, the estimated dynamic correlations at 295 time points were concatenated across 479 subjects, which resulted in $295 \cdot 479 = 141305$ total number of correlations that served as the input to k -means clustering. In numerical implementation of k -means clustering, we repeated clustering 1000 times with different initial centroids and chose the best result with the lowest sum of squared distances. The clustering results are shown in Figure 3, where the heat kernel method has the least number of state changes, i.e., transitions.

3.4. Validation

We validated the proposed method in simulation studies with ground truths. Assume there are 50 subjects, and each subject has two time series x_i and y_i of $n = 295$ data points. We first assigned the ground truth of state space for each subject. For a small number of transitions, we divided the 295 time points into 10 segments assigned with same state randomly chosen from States 1, 2 and 3. We further assumed there is no transition between States 1 and 3 according to the transition probability of real data (Figure 7). We simulated x_i as identical and independently distributed multivariate normal across i , i.e., $x_i \sim N(0, I_n)$. Let $y_i = x_i$ for State 1 and $y_i = -x_i$ for State 1 which give correlation values 1 and -1 respectively. For State 2, let $y_i \sim N(0, I_n)$ independent to x_i for correlation near 0. Then, we computed the dynamic correlation between noisy time series $x_i + N(0, \sigma I_n)$ and $y_i + N(0, \sigma I_n)$ by three methods and applied the k -means clustering. The accuracy, given by the fraction of the estimated state equals to the ground truth, is shown in Figure 4. The MALAB code for obtaining the simulation result (Figure 4) is given in <http://brainimaging.waisman.wisc.edu/~chung/circle>.

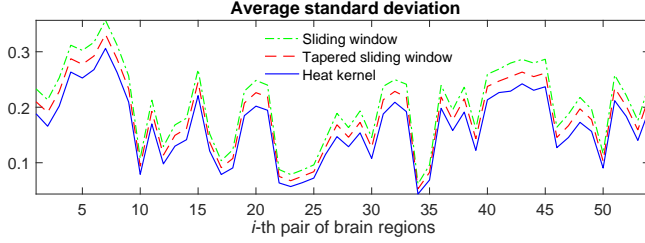


Fig. 5. The average standard deviation of the dynamic correlations over 479 subjects for each interhemispheric pair. From the SW-method, the average standard deviation is reduced between 7.1% and 14.6% by the TSW-method and reduced between 14.2% and 29.5% by the heat kernel method.

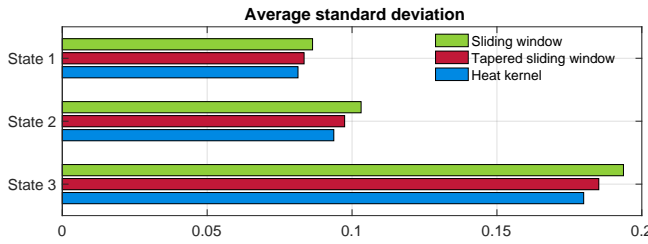


Fig. 6. Average standard deviation within each state over all interhemispheric pairs of regions. From the SW-method, the average standard deviations are reduced by 3.4%, 5.5%, and 4.4% in the TSW-method, and reduced by 5.8%, 9.1%, and 7.1% in the heat kernel method.

3.5. Results

Variability in each interhemispheric pair. For each interhemispheric pair, we averaged the standard deviations of the dynamic correlations over 479 subjects. From the SW-method, the average standard deviation is reduced between 7.1% and 14.6% by the TSW-method, and reduced between 14.2% and 29.5% by the heat kernel method (Figure 5).

Within state variability. We also computed the standard deviations of the correlations within each state and averaged them across 54 interhemispheric pairs. The results are displayed in Figure 6. From the SW-method, the average standard deviations are reduced 3.4%, 5.5%, and 4.4% by the TSW-method, and reduced 5.8%, 9.1%, and 7.1% by the heat kernel method.

Transition probability. The state transitions can reveal the interactions between different brain states. They can be modeled as a Markov chain [21]. For each interhemispheric pair and subject, we computed the transition probability of moving from state i to state j . Figure 7 shows the average transition probability over all subjects and all interhemispheric pairs. The heat kernel method has the lowest transition probabilities between different states and the highest probabilities of remaining in the same state.

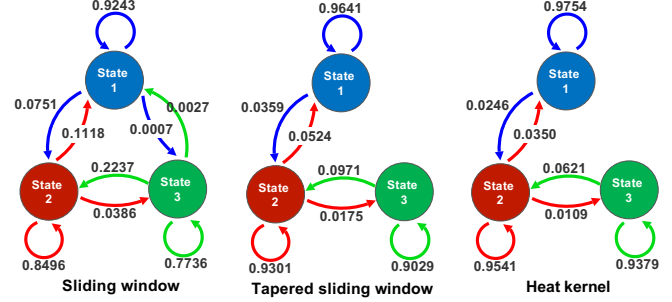


Fig. 7. Transition probabilities averaged across all subjects and interhemispheric pairs. The heat kernel method has the lowest transition probabilities between different states and the highest probabilities of remaining in the same state.

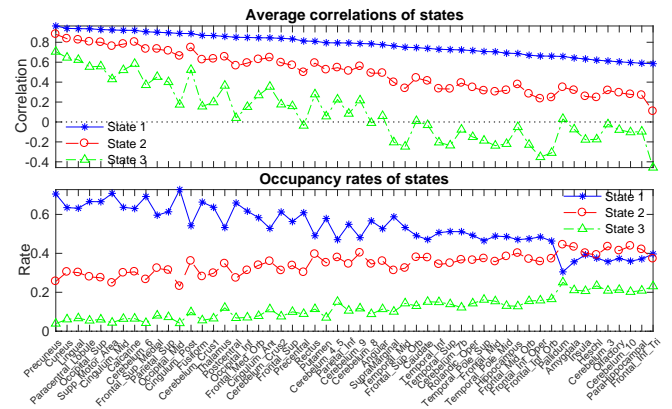


Fig. 8. Top: the average correlations of the three states in order of the values of the average correlations of State 1. Bottom: the occupancy rates of the three states.

Figure 8 shows the average correlation and the occupancy rate [20] of each state and interhemispheric connectivity. The results are displayed in the descending order of correlation in the most dominating state (State 1). Precuneus, cuneus, lingual gyrus, paracentral lobule and superior occipital are the five brain regions having the highest interhemispheric correlations in the state space, and thus have the strongest symmetry compared to other brain regions. The inferior frontal gyrus (pars triangularis), parahippocampal gyrus, lobule X of cerebellar hemisphere, olfactory cortex and lobule III of cerebellar hemisphere are the five brain regions having the weakest interhemispheric symmetry.

Acknowledgement. This study was supported by NIH research grants EB022856, MH101504, P30HD003352, U54HD09025 and UL1TR002373. We would like to thank Siti Balqis Samdin, Chee-Ming Ting and Hernando Ombao of KAUST and Martin Lindquist of JHU for providing valuable discussion and support.

4. REFERENCES

- [1] R.M. Hutchison and J.B. Morton, "Tracking the brain's functional coupling dynamics over development," *Journal of Neuroscience*, vol. 35, no. 17, pp. 6849–6859, 2015.
- [2] R. Hindriks, M.H. Adhikari, Y. Murayama, M. Ganzetti, D. Mantini, N.K. Logothetis, and G. Deco, "Can sliding-window correlations reveal dynamic functional connectivity in resting-state fMRI?," *NeuroImage*, vol. 127, pp. 242–256, 2016.
- [3] A. Kucyi and K.D. Davis, "Dynamic functional connectivity of the default mode network tracks daydreaming," *NeuroImage*, vol. 100, pp. 471–480, 2014.
- [4] E.A. Allen, E. Damaraju, S.M. Plis, E.B. Erhardt, T. Eichele, and V.D. Calhoun, "Tracking whole-brain connectivity dynamics in the resting state," *Cerebral Cortex*, vol. 24, no. 3, pp. 663–676, 2014.
- [5] S. Shakil, C.-H. Lee, and S.D. Keilholz, "Evaluation of sliding window correlation performance for characterizing dynamic functional connectivity and brain states," *NeuroImage*, vol. 133, pp. 111–128, 2016.
- [6] M.A. Lindquist, Y. Xu, M.B. Nebel, and B.S. Caffo, "Evaluating dynamic bivariate correlations in resting-state fMRI: a comparison study and a new approach," *NeuroImage*, vol. 101, pp. 531–546, 2014.
- [7] D.A. Handwerker, V. Roopchansingh, J. Gonzalez-Castillo, and P.A. Bandettini, "Periodic changes in fMRI connectivity," *NeuroImage*, vol. 63, no. 3, pp. 1712–1719, 2012.
- [8] B. Rashid, E. Damaraju, G.D. Pearlson, and V.D. Calhoun, "Dynamic connectivity states estimated from resting fMRI identify differences among schizophrenia, bipolar disorder, and healthy control subjects," *Frontiers in Human Neuroscience*, vol. 8, pp. 897, 2014.
- [9] A.V. Oppenheim, R.W. Schaffer, and J.R. Buck, *Discrete-time signal processing*, Upper Saddle River, NJ: Prentice Hall, 1999.
- [10] M.C. Jones, "Simple boundary correction for kernel density estimation," *Statistics and Computing*, vol. 3, no. 3, pp. 135–146, 1993.
- [11] M.K. Chung, N. Adluru, J.E. Lee, M. Lazar, J.E. Lainhart, and A.L. Alexander, "Cosine series representation of 3D curves and its application to white matter fiber bundles in diffusion tensor imaging," *Statistics and Its Interface*, vol. 3, pp. 69–80, 2010.
- [12] M.K. Chung, K.M. Dalton, L. Shen, A.C. Evans, and R.J. Davidson, "Weighted Fourier representation and its application to quantifying the amount of gray matter," *IEEE Transactions on Medical Imaging*, vol. 26, pp. 566–581, 2007.
- [13] C.A. Burghy, M.E. Fox, M.D. Cornejo, D.E. Stodola, S.L. Sommerfeldt, C.A. Westbrook, C. Van Hulle, N.L. Schmidt, H.H. Goldsmith, R.J. Davidson, et al., "Experience-driven differences in childhood cortisol predict affect-relevant brain function and coping in adolescent monozygotic twins," *Scientific Reports*, vol. 6, pp. 37081, 2016.
- [14] N. Tzourio-Mazoyer, B. Landeau, D. Papathanassiou, F. Crivello, O. Etard, N. Delcroix, B. Mazoyer, and M. Joliot, "Automated anatomical labeling of activations in spm using a macroscopic anatomical parcellation of the MNI MRI single-subject brain," *NeuroImage*, vol. 15, pp. 273–289, 2002.
- [15] A.D. Barber, M.A. Lindquist, P. DeRosse, and K.H. Karlsgodt, "Dynamic functional connectivity states reflecting psychotic-like experiences," *Biological Psychiatry*, vol. 3, no. 5, pp. 443–453, 2018.
- [16] Z. Yang, R.C. Craddock, D.S. Margulies, C.-G. Yan, and M.P. Milham, "Common intrinsic connectivity states among posteromedial cortex subdivisions: Insights from analysis of temporal dynamics," *NeuroImage*, vol. 93, pp. 124–137, 2014.
- [17] A.S. Choe, M.B. Nebel, A.D. Barber, J.R. Cohen, Y. Xu, J.J. Pekar, B. Caffo, and M.A. Lindquist, "Comparing test-retest reliability of dynamic functional connectivity methods," *NeuroImage*, vol. 158, pp. 155–175, 2017.
- [18] H.A. Marusak, V.D. Calhoun, S. Brown, L.M. Crespo, K. Sala-Hamrick, I.H. Gotlib, and M.E. Thomason, "Dynamic functional connectivity of neurocognitive networks in children," *Human Brain Mapping*, vol. 38, no. 1, pp. 97–108, 2017.
- [19] B. Rashid, M.R. Arbabshirani, E. Damaraju, M.S. Cetin, R. Miller, G.D. Pearlson, and V.D. Calhoun, "Classification of schizophrenia and bipolar patients using static and dynamic resting-state fMRI brain connectivity," *NeuroImage*, vol. 134, pp. 645–657, 2016.
- [20] M. Yaesoubi, E.A. Allen, R.L. Miller, and V.D. Calhoun, "Dynamic coherence analysis of resting fMRI data to jointly capture state-based phase, frequency, and time-domain information," *NeuroImage*, vol. 120, pp. 133–142, 2015.
- [21] W.R. Gilks, S. Richardson, and D. Spiegelhalter, *Markov chain Monte Carlo in practice*, Chapman and Hall/CRC, 1995.